Hindawi
International Journal of Electrochemistry
Volume 2020, Article ID 5620530, 10 pages
https://doi.org/10.1155/2020/5620530

Research Article

Synthesis, Electrochemical, Thermodynamic, and Quantum Chemical Investigations of Amino Cadalene as a Corrosion Inhibitor for Stainless Steel Type 321 in Sulfuric Acid 1M

Y. Koumya,[1] **R. Idouhli**,[1] **A. Oukhrib**,[2] **M. Khadiri**,[1] **A. Abouelfida**,[1] **and A. Benyaich**[1]

[1]*Laboratory of Applied Chemistry and Biomass, Department of Chemistry, University Cadi Ayyad, Faculty of Science Semlalia, BP 2390, Marrakech, Morocco*
[2]*Biomolecular Chemistry, Natural Substances and Reactivity Laboratory, Department of Chemistry, Faculty of Sciences Semlalia, University of Cadi Ayyad, BP 2390, Marrakech, Morocco*

Correspondence should be addressed to Y. Koumya; koumya.yassine@gmail.com

Received 24 October 2019; Accepted 11 August 2020; Published 26 August 2020

Academic Editor: Sergio Ferro

The corrosion of stainless steel is one of the major industries' issues that gained wide interest among researchers. It became necessary to develop and apply eco-friendly approaches to corrosion control. This work explores the inhibitory effect of a newly synthesized amino cadalene (ACM) on the corrosion of stainless steel type 321 in sulfuric acid 1M. Particularly, the experimental study consisting of electrochemical and surface analyses was conducted in conjunction with a theoretical approach. The electrochemical results showed that ACM acted as a mixed-type corrosion inhibitor and the inhibition efficiency attained 91% at 10^{-3}M. EIS measurements revealed that both metal charge transfer and diffusion processes are involved in the interfacial metal/solution reactions. The interfacial mechanism is thoroughly investigated; the physisorption of the protonated molecules was preceded by the formation of a negative layer due to adsorption of the solution anionic species. The experimental insights are corroborated with the quantum chemical calculations.

1. Introduction

Stainless steel is a very corrosion-resistant material that is widely used in many industrial applications. In particular, it is largely employed as a material of choice for the chemical industry in aggressive environments, i.e., petroleum refining, chemical processes, and desalination [1]. Due to the chromium content, stainless steel forms a chromium oxide film that gives it the passivity character [2]. In spite of all the encouraging properties, in some environments, the resistance of the passive film is often limited notably in the acidic media. Sulfuric acid has considerable uses covering nearly most industries, such as fertilizer industries, petroleum refinery, paint industry, steel pickling, and extraction of nonmetals [3]. So, the search and application for new and efficient corrosion inhibitors become an obligation to prevent corrosion problems [4]. The use of organic inhibitors is one of the most practical methods for the protection of the materials against the aggressiveness of the acidic media. Furthermore, the effectiveness of these compounds containing heteroatoms, such as S, N, and O, and π electrons is extensively discussed in the literature [5, 6]. As such, they have been considered as efficient inhibitors for their ability in establishing the adsorption onto the metal surface. Generally, their inhibition efficiency is linked to the polar functions acting as active centers for the adsorption.

Several investigations have been interested in the inhibition of the corrosion of metals by using the natural plant extracts, such as the sesquiterpenes of the essential oil of different plants that are of great interest. Besides that, the need for organic molecules having a particular structure and properties for different uses has prompted the need to synthesize new products from sesquiterpenes and their derivatives [7]. Cadalene is a dehydrogenation molecule of

some sesquiterpenes contained in the essential oil [8]. In addition, the amino cadalene molecule (ACM) is a new cadalene product that is derived from the bicyclic sesquiterpenes, α- and β-himachalene, which are the main constituents of the essential oil of the Atlas cedar plant (Cedrus Atlantica) [9]. A previous study on the corrosion inhibition of steel in hydrochloric acid has shown that sesquiterpene molecules are efficient corrosion inhibitors [10]. As has been discussed by different authors, these compounds meet the criteria demanded for the corrosion inhibitors [11, 12]. In this context, the efficiency of the sesquiterpenes and their derivatives has sparked our interest in investigating the effect of these molecules on the corrosion behavior of the stainless steel.

The present work investigates the inhibitory effect of ACM on the corrosion behavior of stainless steel (SS) in sulfuric acid. The inhibition efficiency was studied by using the potentiodynamic polarization and the electrochemical impedance spectroscopy (EIS). To explore even more the inhibition mechanism, scanning electron microscopy (SEM) was used to observe the surface morphology. Quantum chemical calculations were performed to study the inhibitor active centers responsible for the adsorption process and to determine the link between the inhibition properties and the molecular structure of the inhibitor. The corrosion behavior of stainless steel in sulfuric acid as well as the inhibition investigation was done on AISI type 321 SS which is the most used alloy in the refinery unit processing heavy crude oil [13].

2. Experimental

2.1. Electrodes and Materials. The working electrode was cut from the AISI type 321 SS sheet; the chemical composition (wt. %) provided by the manufacturer is given in Table 1. The samples were cut into a rectangular shape with a dimension of 1.2 cm × 0.8 cm; then, the specimens were sealed by epoxy resin leaving an exposed area of 0.96 cm^2. The stainless steel electrode was first polished successively with silicon carbide emery paper (SiC) of increasing fineness, i.e., 500, 1200, 1500, and 2000 grits.

Then, they were washed with distilled water, rinsed with acetone, and dried in air for the use in electrochemical measurements. Sulfuric acid (1M H_2SO_4) was prepared by dilution of analytical H_2SO_4 (97%) with distilled water. A volume of 80 mL of diluted sulfuric acid was used to ensure the proper immersion of electrodes in the cylindrical Pyrex glass cell. A three-electrode conventional cell, consisting of 321 SS working electrode (WE), a platinum counter electrode (CE), and a saturated calomel electrode (SCE) as a reference electrode, was used for measurements. In order to perform the EIS experiments at a steady state, the stirrer rotational speed was set at 180 rpm and at a controlled temperature of 293 K using a bath thermostat.

2.2. Electrochemical Tests. The electrochemical measurements were carried out using laboratory potentiostat (voltalab PGZ 301). Polarization curves were recorded at a constant sweep rate of 1 mV/s, and the scanning range was from −600 mV versus SCE to 0 mV versus SCE. Before each experiment, the working electrode was immersed in the test cell for 60 min until attaining a steady state. The measurements were repeated three times for each condition to ensure reproducibility. EIS measurements were carried out in a frequency range of 100 kHz to 10 MHz with an amplitude of 10 mV peak-to-peak using alternating current (AC) signals at open circuit potential (OCP). Double-layer capacitance (C_{dl}) and charge transfer resistance (R_{ct}) values were obtained from EIS measurements.

Table 1: Chemical composition (wt. %) of AISI SS type 321.

Fe	Cr	Ni	Ti	Si	Mn	P	S	N
Balance	17–19	9–12	0.3–0.7	0.75	2.00	0.045	0.03	0.10

2.3. Synthesis of Amino Cadalene. The bicyclic sesquiterpenes, α- and β-himachalene, are the main constituents of the essential oil of the Atlas cedar (Cedrus Atlantica). The catalytic dehydrogenation of the mixture of α- and β-himachalene by 5% of palladium on carbon (10%) at high temperature (553 K) gives, with good yield, the mixture of aryl himachalene and 1-isopropyl- 4,7-dimethylnaphthalene with respective proportions of 64/36. Treatment of the 1-isopropyl-4,7-dimethylnaphthalene by a mixture of nitric acid and sulfuric acid in dichloromethane at 26°C for 2 hours gives the nitro compound with a yield of 70%. Then, the corresponding amine-cadalene was obtained by hydrogenation of the obtained nitro compound with HCl/Zn in dichloromethane at room temperature for 6 h to afford **4** with an 80% yield. The structure of amino cadalene was then confirmed by NMR data. Figure 1 shows the different steps of amino cadalene synthesis.

^{1}H NMR (300 M*Hz*, Chloroform-*d*) δ 7.92 (d, $J = 8.6$ *Hz*, 1H), 7.99 (s, 1H), 7.29 (s, 2H), 7.20 (s, 1H) 6.05 (d, $J = 8.6$ *Hz*, 1H), 3.80 (hept, $J = 6.9$ *Hz*, 1H), 2.72 (s, 3H), 2.63 (s, H), 1.46 (d, $J = 6.8$ *Hz*, 6H). ^{13}C NMR (75 M*Hz*, $CDCl_3$) δ 148.27 (Cq), 139.25(Cq), 133.92(Cq), 129.87(Cq), 129.15(Cq), 128.85(Cq), 126.94 (CH), 123.95 (CH), 122.98 (CH), 121.16 (CH), 27.98 (CH_{isPr}), 23.15 ($(CH_3)_2$), 21.72 (CH_3), 18.87 (CH_3).

3. Results

3.1. Potentiodynamic Polarization. The effect of the inhibitor concentration on the corrosion behavior of SS was studied by using potentiodynamic polarization. Figure 2 shows the potentiodynamic polarization curves for AISI 321 SS in 1M H_2SO_4 containing different concentrations of ACM. The evaluated parameters of polarization curves including corrosion potential (E_{corr}), corrosion current density (i_{corr}), cathodic Tafel constant (β_c), and the inhibition efficiency (η) are summarized in Table 2. The corrosion current density (i_{corr}) was obtained by extrapolating the linear segments of the cathodic Tafel curve to the corrosion potential (E_{corr}).

The inhibition efficiency η (%) was calculated by

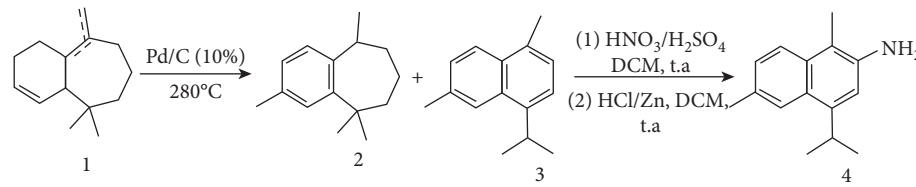

Figure 1: Scheme for synthesis of ACM.

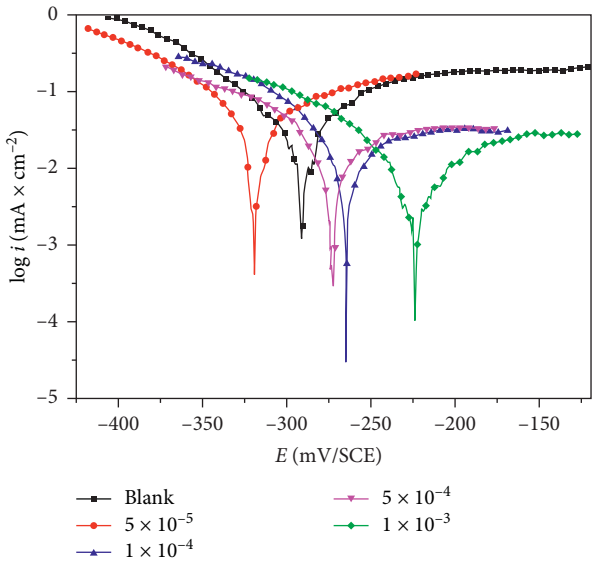

Figure 2: Potentiodynamic polarization for SS in 1M H_2SO_4 containing different concentrations of ACM at 293 K.

Table 2: Tafel polarization parameters and corresponding inhibition efficiency for SS in 1M H_2SO_4 containing different concentrations of ACM at 293 K.

Conc. (M)	E_{corr} (mV versus SCE)	i_{corr} (μA/cm^2)	β_c (mV/dec)	η (%)
Blank	−292	169.70	−147	—
5×10^{-5}	−319	66.75	−92	60.66
1×10^{-4}	−264	44.92	−116	73.53
5×10^{-4}	−272	34.77	−126	79.51
1×10^{-3}	−224	15.20	−89	91.04

$$\eta(\%) = \frac{i_{corr} - i_{corr(inh)}}{i_{corr}} \times 100, \quad (1)$$

where i_{corr} and $i_{corr\ (inh)}$ are corrosion current density without and with the addition of inhibitor, respectively. The curves show that the added ACM acts on both anodic and cathodic branches of the polarization curve, which indicates that both anodic metal dissolution and cathodic reduction reactions were inhibited. Besides, the corrosion potential was shifted toward the positive direction as the concentration of ACM increased. Some authors have reported that an inhibitor can be classified as a mixed type if the change of corrosion potential is less than 85 mV with respect to the corrosion potential of the blank [14]. As observed from the parameters depicted in Table 2, the maximum shift was about 68 mV in the case of the concentration 10^{-3}M of ACM, which confirms the mixed character of the inhibitor. It is reasonable to assume that the present ACM acts significantly on both the anodic dissolution and cathodic reactions. Additionally, the decrease in the cathodic slope with the increase in the ACM concentration indicates that the cathodic sites of hydrogen evolution were blocked by the adsorbed inhibitor species [15]. Also, it is apparent that corrosion current density decreases considerably as soon as the inhibitor is added. Furthermore, the inhibition efficiency was found to increase as ACM concentration increases. The maximum inhibition efficiency was about 91% for 10^{-3}M of ACM.

3.2. Electrochemical Impedance Spectroscopy. Nyquist plots for AISI 321 SS in 1M sulfuric acid with and without various concentrations of ACM are given in Figure 3. Parameters derived from Nyquist plots are listed in Table 3.

The inhibition efficiency is calculated by the following equation:

$$\eta(\%) = \frac{R'_{ct} - R_{ct}}{R_{ct}} \times 100, \quad (2)$$

where R_{ct} and R'_{ct} are, respectively, charge transfer resistances in the absence and presence of the inhibitor.

For better visualization of the inflection points of the impedance module as well as the phase angle variation, the Bode plotting is preferred. Additionally, it makes it possible to discern the different time constants. Bode plots of SS in sulfuric acid without and with different concentrations of ACM are shown in Figure 4. These plots demonstrate the effect of the ACM concentration on the corrosion behavior of SS in the aggressive medium. The Nyquist plots shown have the same shape; also, all depicted graphs show two time constants. The capacitive loop at the high frequencies is generally attributed to the charge transfer process and the electric double layer [16]. However, the straight lines observed at lower frequencies represent the Warburg tail which indicates that the diffusion of the species through the passive film is the step limiting of its dissolution [17]. Therefore, it is reasonable to assume that both charge transfer and diffusion processes are controlling the dissolution of the SS.

It is clearly evident from Figure 3 and Table 3 that increasing the concentration of ACM in the sulfuric acid increases the charge transfer resistance. This indicates that due to the inhibitor adsorption on the metal surface, the interface becomes more resistant to the charge transfer as the concentration of the ACM increases [18]. The inhibition efficiency attains 87% at 10^{-3}M of ACM. On the other hand, the decrease in the double layer capacitance with the increase

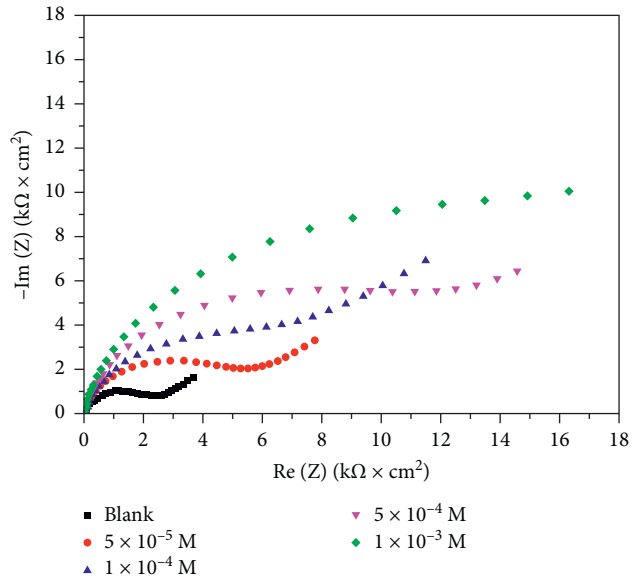

Figure 3: Nyquist plots for SS in 1M H_2SO_4 containing different concentrations of ACM at 293 K.

Table 3: EIS parameters for SS in 1M H_2SO_4 containing different concentrations of ACM at 293 K.

Conc. (M)	R_s ($\Omega \times cm^2$)	R_{ct} ($k\Omega \times cm^2$)	C_{dl} ($\mu F/cm^2$)	η (%)
Blank	0.22	2.17	81.35	—
5×10^{-5}	1.01	4.99	65.16	56.47
1×10^{-4}	0.97	6.40	73.61	66.06
5×10^{-4}	0.96	11.15	72.05	80.52
1×10^{-3}	1.03	16.93	46.46	87.17

of the amount of the inhibitor may be attributed to the replacement of the water molecules by adsorbed ACM, resulting in a decrease in the local dielectric constant of the interface [19]. Besides, Bode plots depicted in Figure 4 show that the value of the impedance in the inhibited solution is larger than the blank solution. Additionally, it is observed from the Bode phase plot that the maximum of the phase angle in the presence of the inhibiter is higher than that of the blank, which indicates the good inhibition performance of ACM. It is clearly observed from both impedance presentations that the inhibitor increases the impedance without changing the aspects of the corrosion process. Also, it is worth adding that both electrochemical impedance and polarization measurements show the same trend.

3.3. Adsorption Isotherm. The process of the inhibitor adsorption on the metal surface is the main step justifying its inhibition efficiency. Hence, the strong adsorption of the inhibitor on the metal surface results most frequently in significant decrease in the corrosion current density. The fit of the obtained results could give further information on the nature of the ACM interaction with the SS surface. To achieve this, we have made different attempts to fit the

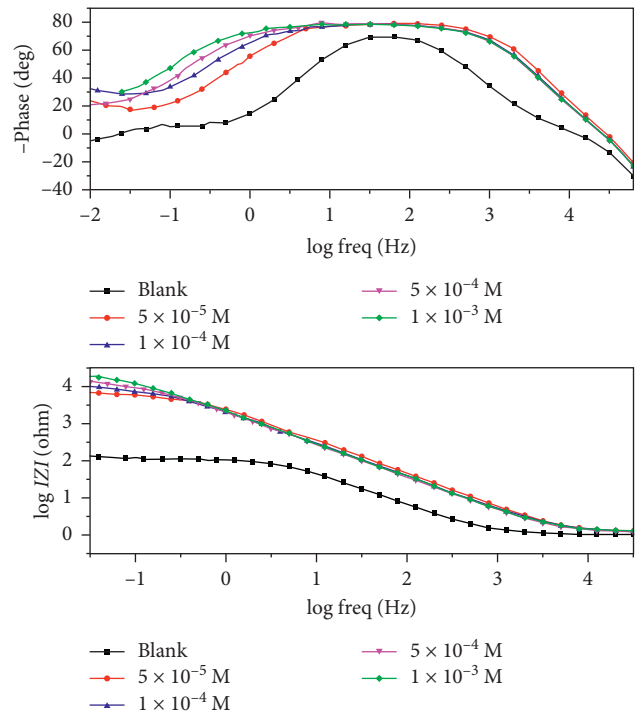

Figure 4: Bode diagram for SS in 1M H_2SO_4 in the absence and presence of different concentrations of ACM at 293 K.

empirical values to different isotherms. The surface coverage and the inhibitor concentration were fitted to different adsorption isotherms (Langmuir, Freundlich, and Temkin). The adsorption data listed in Table 4 reveals that the adsorption of ACM on the SS surface fits well with Langmuir isotherm ($R^2 = 0.995$). It is worth adding that the Langmuir isotherm is based on the assumption that the inhibitor adsorption is monolayer with no lateral interaction between the adsorbed species [20, 21].

The surface coverage (θ) and the standard free energy (ΔG°) were calculated following the procedure described elsewhere [20]. The values of standard free energy and correlation coefficient for different adsorption isotherms are listed in Table 4. The negative sign of ΔG° values suggests the spontaneous adsorption of ACM on the SS surface [22]. Generally, if $-\Delta G^\circ$ value is between 20 kJ/mol and 40 kJ/mol, it represents both physisorption and chemisorption [17]. The calculated ΔG° value for Langmuir isotherm is about −34.442 kJ/mol; thus, the adsorption of ACM on the SS implies both electrostatic interaction between the charged molecules and the charged metal and charge sharing between the ACM and the metal surface.

3.4. Thermodynamic Parameters. The temperature of the corrosive medium is one of the factors affecting the inhibition mechanism. Effective inhibitors are expected to perform under a wide range of conditions. Hence, a special focus must be paid to the selection of inhibitors performing for various practical applications [23]. In this context, we tried to examine the kinetic behavior of stainless steel in sulfuric acid at various temperatures for both cases of

Table 4: Parameters derived from adsorption models and coefficients of determination at 293 K.

Isotherm	R^2	Slope	Intercept	K_{ads}		ΔG°_{ads} (kJ/mol)
Langmuir	0.995	1.079	4×10^{-5}	25.103	—	−34.442
Temkin	0.912	0.087	1.493	1.0173	b_T 27.986	−9.822
Freundlich	0.902	0.116	0.300	1.9952	n 0.116	−11.463

inhibition with and without ACM. Potentiodynamic polarization measurements of SS in sulfuric acid without and with inhibitor were conducted at different temperatures in order to explain the change in the stability of adsorbed inhibitor. Table 5 shows the parameters derived from potentiodynamic polarization measurements of the corrosion of the SS for different temperatures. It is clearly noticed that the corrosion current density rises sharply with the increase in temperature. The inhibition efficiency was found to decrease as the temperature increases from 293 K to 323 K. Thus, the temperature affects considerably the strength of the adsorption. Therefore, the observed features can be explained by the physical adsorption of the inhibitor on the metal surface [24].

The determination of the activation energy E_a and enthalpy and entropy of activation (ΔH_a^*, ΔS_a^*) from Arrhenius equations can be found in detail elsewhere [10, 24–27] and is summarized in Table 6. Figure 5 shows the plot of ln (i_{corr}) against $1/T$ in the absence and presence of inhibitor; from the slope ($-E_a/R$), the value of the apparent activation energy is determined. It is clearly shown in Table 6 that the value of apparent activation energy in the presence of the inhibitor is higher than its value for the blank medium. The increase in E_a in the presence of an inhibitor with respect to the blank solution means the physical adsorption of the ACM on the SS surface. According to Szauer et al., the increase in activation energy could be attributed to an appreciable decrease in the adsorption of the inhibitor upon the temperature increase [28]. Since the processes of adsorption and desorption of inhibitor are in equilibrium, the less the inhibitor is adsorbed onto the metal surface, the more the desorption of inhibitor occurred.

Figure 6 shows a plot of ln (i_{corr}/T) versus $1/T$. A straight line is obtained with a slope of ($\Delta H_a^*/R$) and an intercept of ln (R/hN) + ($\Delta S/R$) from which the values of ΔS_a^* and ΔH_a^* are calculated. From the obtained data, the positive sign of ΔH_a^* for both uninhibited and inhibited solutions indicates the endothermic nature of SS dissolution [29]. We can notice that E_a and ΔH_a^* values vary in the same way which verifies the thermodynamic equation between the E_a and ΔH_a^* as presented in Table 6.

It is generally agreed that the adsorption of inhibitor on the metal surface is an exothermic process accompanied by a decrease in entropy due to the quasi-substitution between the inhibitor molecules from the aqueous solution and the water molecules at the electrode surface.

The values of entropy in the absence and presence of inhibitor are listed in Table 6. The positive sign of entropy in the presence of an inhibitor suggests that the adsorption process is accompanied by an increase in entropy. This fact might be explained as follows: the adsorption of organic inhibitor is accompanied by the desorption of water molecules from the surface. Also, the obtained value of entropy is considered as an algebraic sum of the solvent desorption and inhibitor adsorption. In the meantime, while inhibitor adsorption is considered to be associated with a decrease in entropy of solute, the water molecules desorption is believed to be associated with an increase in entropy. Thus, the increase in entropy is associated with an increase in solvent entropy. Therefore, the more the solvent entropy increases, the more the inhibitor adsorption will occur [30]:

$$E_a - \Delta H_a^* = RT. \tag{3}$$

3.5. Scanning Electron Microscopy. Scanning electron microscopy (SEM) characterization was used in order to differentiate the surface morphology obtained under different conditions of immersion. Besides that, the local composition of each surface was determined using the EDS analysis. Figure 7(a) shows the surface state of freshly polished SS specimen; it shows a very smooth surface that presents some scratches due to the mechanical polishing. The SEM image in Figure 7(b) shows the damage incurred by the aggressive medium resulting in the observed corrosion product spots. Figure 7(c) shows the surface morphology of SS in an inhibited solution containing 10^{-3}M of ACM. This figure undoubtedly evinces the adsorption of the ACM on the SS with a random distribution. It is clearly observed (Table 7) that after immersion in the aggressive medium, the iron and chromium contents are reduced compared to the freshly polished specimen, which confirms the dissolution of the SS after immersion. After exposure to the inhibited medium, the increase in O and C percentages lends support to the inhibitor adsorption on the metal surface.

3.6. Quantum Chemical Studies. The geometric optimization of ACM and the quantum chemical calculations are carried out using the density functional theory (DFT). DFT is presently considered the most successful theory to study the mechanism of the inhibition based on the structural nature of molecules [31]. Besides, it provides deep insights into the molecular properties of the inhibitor. ACM was built with the Gauss View software 09W and then has been optimized using the hybrid method of B3LYP function with a 6-31G (d, p) basis set [32].

In the present study, the DFT quantum calculations were used to correlate the molecular structure and the inhibition

Table 5: Polarization measurements for SS without and with ACM (10^{-3}M) for different temperatures.

	T (K)	i_{corr} ($\mu A \times cm^{-2}$)	E_{corr} (mV versus SCE)	β_c (mV/dec)	η (%)
Blank	293	169.7	−292	−147.7	—
	303	475.0	−371	−143.1	—
	313	744.4	−376	−152.1	—
	323	1123	−319	−120.9	—
Inhibitor	293	15.19	−224	−89.8	91.04
	303	120.71	−348	−117.6	74.58
	313	466.8	−332	−100.2	37.29
	323	941.6	−316	−99.4	16.15

Table 6: Activation data of SS dissolution in 1M H_2SO_4 without and with ACM.

	E_a (kJ/mol)	ΔH°_{ads} (kJ/mol)	ΔS°_{ads} (J/mol × K)	$E_a - \Delta H^\circ_{ads}$
Blank	48.43	45.86	−44.23	2.5
Inhibitor	108.66	106.08	142.42	2.5

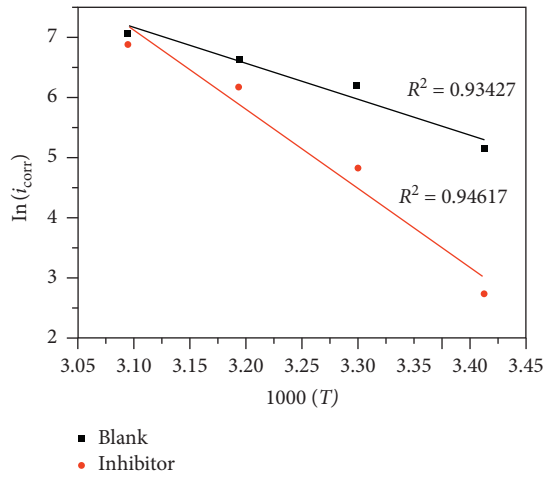

Figure 5: Arrhenius plots for SS in 1M H_2SO_4 in the absence and presence of 10^{-3}M of ACM.

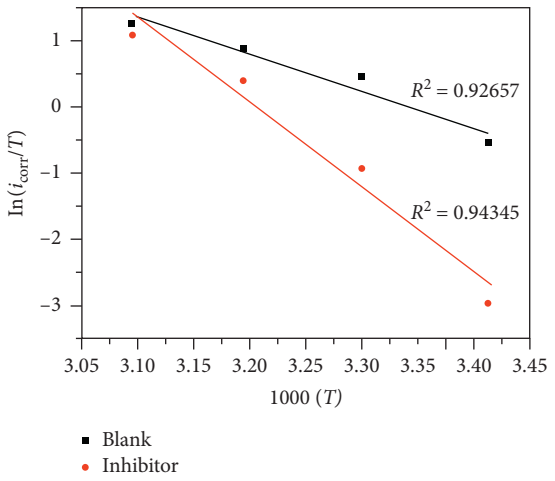

Figure 6: Transition-state plots for SS in 1M H_2SO_4 in the absence and presence of 10^{-3}M of ACM.

efficiency observed from obtained experimental data. The different quantum chemical parameters were determined as described elsewhere [33]. The difference between the LUMO and HOMO energy levels of the inhibitor molecule is an important index for the inhibitory potential of a molecule. It is reported that good inhibitors could both donate electrons to the vacant d orbitals of the metal and receive back the electrons from the metal. Also, the low absolute value of the energy bandgap (ΔE) indicates a good inhibition efficiency [31]. Figure 8 shows the optimized structure of amino cadalene, and the corresponding quantum parameters are listed in Table 8.

The fraction of electrons transferred means that the electrons flow transferred from the molecule to the SS surface. Generally, the values of ΔN are strongly related to the electron donation ability which is in turn a crucial index that serves in justifying the observed inhibition efficiency. Table 8 shows that ACM has a higher value of E_{HOMO} and lower E_{LUMO}, with a lower energy bandgap.

According to Lukovits et al. [33], a value of $\Delta N < 3.6$ indicates that the inhibition efficiency could be improved by the increase in the electron-donating ability of the inhibitor [31, 34]. The highest inhibition efficiency observed is not due only to the electron-donating ability, since the value ΔN is higher than 3.6 [31]. The values of the hardness $\eta > 0$ and $\Delta E_T < 0$ suggest that the inhibition efficiency of ACM is due to the charge transfer to a molecule followed by the back donation process. The obtained properties are similar to those reported in the literature [35].

For the purpose of estimating the active centers through which the inhibitor interacts with the metal surface, so it is necessary to investigate the electronic charge of these atoms [36]. The Mulliken population analysis is used to calculate the charge distribution over the whole structure of ACM [37]. It is widely reported in the literature that the inhibition efficiency depends on the presence of electronegative atoms in the molecular structure [4]. Several authors have discussed the relation between the magnitude of the charge and the adsorption ability. Generally, the higher the magnitude

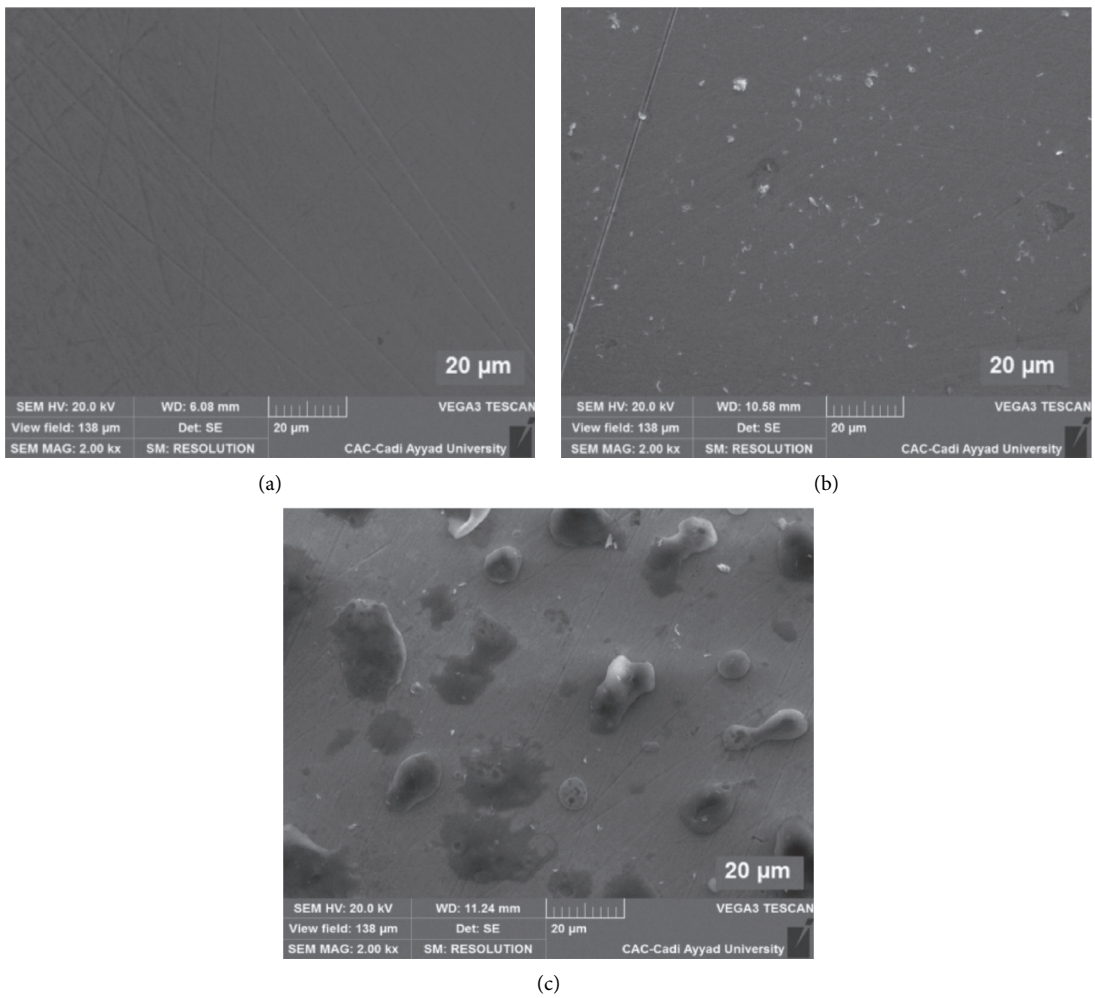

Figure 7: SEM micrographs of (a) freshly polished SS specimen, (b) SS specimen exposed to 1M H_2SO_4, and (c) SS specimen exposed to 1M H_2SO_4 containing 10^{-3}M of ACM.

of the negative charge of the heteroatom, the higher its ability to be adsorbed on the metal surface via the donor acceptor type bond [38].

The Mulliken charge distribution of ACM is presented in Table 9. It is clear that the highest negative charge is found on the nitrogen atom (−0.824) as well as some carbon atoms indicating that these are the active sites for the electrophilic attack [39]. Furthermore, the carbon atoms that carry positive charges are considered as the sites to which nucleophiles can attack [38].

The local reactivity of ACM can be studied by the calculation of the Fukui indices [40]. Parr and Yang proposed that the larger value of Fukui function [29] corresponds to the more reactive active center in the molecule. So, the Fukui function allows computing the local reactivity indices and estimating each molecular contribution. These indices can be determined as described elsewhere [41].

Usually, the highest value of f_k^+ corresponds to the most probable nucleophilic attack site while the highest f_k^- corresponds to the most probable electrophilic attack site [42]. The highest Fukui indices of ACM are presented in Table 9. The most reactive sites for both nucleophilic and electrophilic attacks are 19N, 15C, 22C, 28C, and 32C, since they have the highest nucleophilic and electrophilic Fukui indices.

3.7. Potential of Zero Charge. The adsorption mechanism of the organic molecules is highly influenced by the charge of the metal surface [43]. In order to discuss the possible interactions between the ACM and the metal surface, the surface charge of SS was studied by determining the potential of zero charge (PZC) which is the potential where the solution side of the double layer does not have any charge [44]. The PZC was measured by carrying out the EIS measurements at different potentials other than corrosion potential. The double-layer capacitance for the SS in 1M sulfuric acid containing the optimum concentration of ACM was calculated and plotted for different potentials as shown in Figure 9. It is clearly observed that the capacitance value decreases as the potential tends to more positive values, then attains a minimum capacitance at 500 mV versus SCE, and rises again with more anodic potentials. The nature of the

Table 7: Weight percentage of SS alloying elements of (a) freshly polished specimen surface, (b) exposed to 1M H_2SO_4, and (c) exposed to 1M H_2SO_4 containing 10^{-3}M of ACM.

Elements	Weight (%)		
	(a)	(b)	(c)
C	02.19	02.03	29.69
O	01.19	01.11	02.14
Cr	17.58	17.33	12.16
Fe	69.10	67.20	47.20

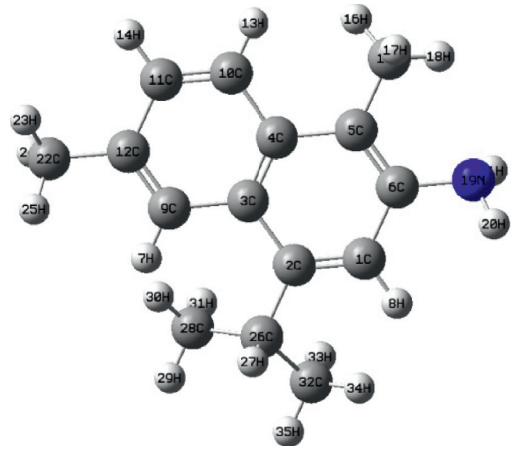

Figure 8: Optimized structure of ACM with the B3LYP/6-31G (d, p).

Table 8: Molecular properties of ACM calculated using DFT at the B3LYP/6-31G (d, p) basis set.

E_{HOMO}	E_{LUMO}	ΔE (eV)	ΔN (eV)	ΔE_T (eV)	μ (D)
−0.17403	−0.01737	0.1566	45.2936	−0.01957	1.8910

Table 9: Mulliken charges and Fukui indices of ACM.

Atom	Mulliken charge	f_k^-	f_k^+
1C	−0.205	−0.296122	−0.217434
2C	0.088	0.090084	0.153727
3C	0.041	0.043488	0.055688
4C	0.019	0.036875	0.036388
5C	0.081	0.037768	0.110354
6C	0.200	0.123649	0.174388
9C	−0.211	−0.279292	−0.179320
10C	−0.173	−0.227862	−0.139367
11C	−0.150	−0.212445	−0.150402
12C	0.119	0.111155	0.121676
15C	0.495	−0.493384	−0.502078
19N	−0.824	−0.797001	−0.720655
22C	−0.484	−0.519184	−0.524307
26C	−0.168	−0.133326	−0.178921
28C	−0.393	−0.413773	−0.449291
32C	−0.403	−0.434435	−0.459154

adsorbed species can be determined by calculating the correlative scale of the potentials as follows [45]:

$$\Phi = E_{corr} - E_{pzc}, \quad (4)$$

where E_{pzc} is the potential of zero charge. The value of E_{corr} SS in sulfuric acid with 10^{-3}M of inhibitor was −224.4 mV versus SCE, and the value of the correlative scale is about

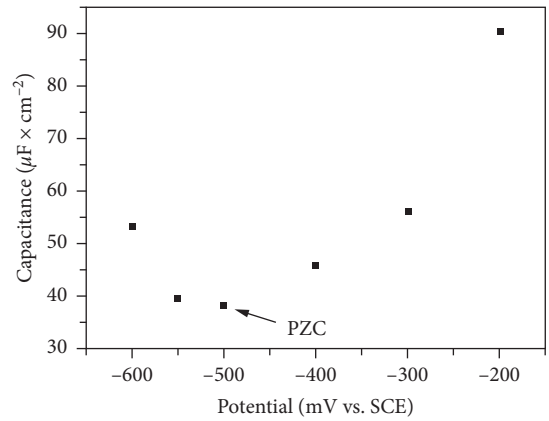

Figure 9: Plot of capacitance against the applied potential for SS in 1M H_2SO_4 containing 10^{-3}M ACM.

+275 mV versus SCE, which meant that the SS surface carried a positive charge. The adsorption mechanism for the positively charged surface has been widely discussed in the literature [46, 47]. Many authors have noted that when the metallic surface is positively charged, the chloride ions and negative species adsorb first on the metal surface [42, 43]. Therefore, the resulting negatively charged surface facilitates the adsorption of the protonated inhibitors through electrostatic attraction [46]. It should be noted that the protonation of the amino functional group of ACM is favorable in sulfuric acid. Hence, after the first adsorption of Cl^- and SO_4^{2-} species, the protonated ACM will adsorb by electrostatic interaction on the first formed layer of the negative species. As mentioned earlier ACM is a mixed adsorption inhibitor that implies both physisorption and chemisorptions. Besides the observed physical adsorption of the protonated molecule, the unprotonated ACM forms coordinate bonds with *d* unoccupied molecular orbitals of metal via lone electron pair of nitrogen atoms. The schematic diagram of the adsorption process is shown in Figure 10. Similar observations were reported by Satpati et al. [44].

4. Conclusion

This work has explored the effect of amino cadalene on the corrosion behavior of 321 stainless steel in sulfuric acid. By combining the electrochemical experiments and quantum chemical calculations, it was possible to thoroughly describe the inhibitor adsorption on the metal surface for different experimental conditions. The potentiodynamic polarization showed that ACM acts as a mixed type inhibitor. The inhibition efficiency has attained a maximum of 91% at 10^{-3}M

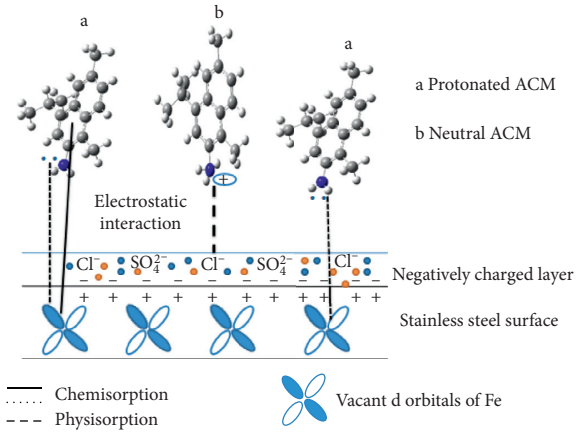

Figure 10: Schematic diagram of the adsorption process of ACM on the SS surface.

depending on the inhibitor concentration and the medium temperature. SEM-EDX analyses confirmed the adsorption of ACM on the SS surface and justified its performance in inhibiting the stainless steel corrosion. The adsorption process was found to be spontaneous and follows Langmuir isotherm; also, the value of free energy was indicative of both chemisorption and physisorption. On the other hand, the quantum chemical calculations showed a good correlation with the experimental results. Fukui indices of ACM revealed that the most probable sites for electrophilic and nucleophilic attacks are 19N, 15C, 22C, 28C, and 32C. Moreover, the PZC data gave more insights on the inhibition mechanism. It was found that the formed layer of the anionic species promotes the adsorption of the protonated ACM.

Data Availability

The data used to support the findings of this study are available within the article. The data are also available from the corresponding author upon reasonable request.

Conflicts of Interest

The authors confirm that there are no conflicts of interest associated with this publication.

References

[1] R. A. Covert and A. H. Tuthill, *Corrosion Mechanisms in Theory and Practice*, vol. 17, CRC Press, Boca Raton, CA, USA, 2002.

[2] A. Pardo, M. C. Merino, A. E. Coy, F. Viejo, R. Arrabal, and E. Matykina, "Pitting corrosion behaviour of austenitic stainless steels—combining effects of Mn and Mo additions," *Corrosion Science*, vol. 50, no. 6, pp. 1796–1806, 2008.

[3] R. T. Loto, C. A. Loto, A. P. I. Popoola, and M. Ranyaoa, "Corrosion resistance of austenitic stainless steel in sulphuric acid," *International Journal of Physical Sciences*, vol. 7, no. 10, pp. 1677–1688, 2012.

[4] T. Ghailane, R. A. Balkhmima, R. Ghailane et al., "Experimental and theoretical studies for mild steel corrosion inhibition in 1M HCl by two new benzothiazine derivatives," *Corrosion Science*, vol. 76, pp. 317–324, 2013.

[5] A. Bimoussa, Y. Koumya, A. Abouelfida et al., "Hemisynthesis, crystal structure and inhibitory effect of sesquiterpenic thiosemicarbazones and thiazolidin-4-ones on the corrosion behaviour of stainless steel in 1M H_2SO_4 solution," *Acta Crystallographica Section C Structural Chemistry*, vol. 75, no. 6, pp. 623–632, 2019.

[6] S. Manimegalai and P. Manjula, "Thermodynamic and adsorption studies for corrosion inhibition of mild steel in aqueous media by Sargasam swartzii (brown algae)," *Journal of Materials and Environmental Science*, vol. 6, no. 6, pp. 1629–1637, 2015.

[7] A. Oukhrib, A. Benharref, M. Saadi, M. Berraho, and L. El Ammari, "(1S,3R,8R,9S,11R)-2,2-dibromo-10,10-dichloro-3,7,7,11-tetramethyltetracyclo[6.5.0.01,3.09,11]tridecane," *Acta Crystallographica Section E Structure Reports Online*, vol. 69, no. 5, p. o724, 2013.

[8] E. de B. Barnett and J. W. Cook, "A new synthesis of cadalene," *Journal of the Chemical Society*, vol. 22, pp. 22–24, 1931.

[9] A. El Haib, A. Benharref, S. Parrès-Maynadié, E. Manoury, M. Urrutigoïty, and M. Gouygou, "Lewis acid- and bronsted acid-catalyzed stereoselective rearrangement of epoxides derived from himachalenes: access to new chiral polycyclic structures," *Tetrahedron: Asymmetry*, vol. 22, no. 1, pp. 101–108, 2011.

[10] R. Idouhli, A. Oukhrib, Y. Koumya, A. Abouelfida, A. Benyaich, and A. Benharref, "Inhibitory effect of atlas cedar essential oil on the corrosion of steel in 1M HCl," *Corrosion Reviews*, vol. 36, no. 4, pp. 373–384, 2018.

[11] M. Znini, "Green approach to corrosion inhibition of mild steel by essential oil leaves of Asteriscus graveolens (forssk.) in sulphuric acid medium," *International Journal of Electrochemical Science*, vol. 7, pp. 3959–3981, 2012.

[12] F. Darriet, "Evaluation of Eryngium maritimum essential oil as environmentally friendly corrosion inhibitor for mild steel in hydrochloric acid solution," *International Journal of Electrochemical Science*, vol. 8, no. 3, pp. 4328–4345, 2013.

[13] H. M. Shalaby, K. Ravindranath, N. Tanoli, and B. Al-Wakaa, "Failure of 321 stainless steel heater tube in heavy crude oil," *Case Studies in Engineering Failure Analysis*, vol. 9, pp. 1–8, 2017.

[14] Q. Hu, Y. Qiu, G. Zhang, and X. Guo, "Capsella bursa-pastoris extract as an eco-friendly inhibitor on the corrosion of Q235 carbon steels in 1 mol·L^{-1} hydrochloric acid," *Chinese Journal of Chemical Engineering*, vol. 23, no. 8, pp. 1408–1415, 2015.

[15] S. Banerjee, V. Srivastava, and M. M. Singh, "Chemically modified natural polysaccharide as green corrosion inhibitor for mild steel in acidic medium," *Corrosion Science*, vol. 59, pp. 35–41, 2012.

[16] M. El Faydy, M. Galai, A. El Assyry et al., "Experimental investigation on the corrosion inhibition of carbon steel by 5-(chloromethyl)-8-quinolinol hydrochloride in hydrochloric acid solution," *Journal of Molecular Liquids*, vol. 219, pp. 396–404, 2016.

[17] P. Thanapackiam, S. Rameshkumar, S. S. Subramanian, and K. Mallaiya, "Electrochemical evaluation of inhibition efficiency of ciprofloxacin on the corrosion of copper in acid media," *Materials Chemistry and Physics*, vol. 174, pp. 129–137, 2016.

[18] A. A. Hermas and M. S. Morad, "A comparative study on the corrosion behaviour of 304 austenitic stainless steel in sulfamic and sulfuric acid solutions," *Corrosion Science*, vol. 50, no. 9, pp. 2710–2717, 2008.

[19] A. Kosari, M. H. Moayed, A. Davoodi et al., "Electrochemical and quantum chemical assessment of two organic compounds

from pyridine derivatives as corrosion inhibitors for mild steel in HCl solution under stagnant condition and hydrodynamic flow," *Corrosion Science*, vol. 78, pp. 138–150, 2014.

[20] R. Idouhli, A. Abouelfida, A. Benyaich, and A. Aityoub, "Cuminum cyminum extract—a green corrosion inhibitor of S300 steel in 1M HCl," *Chemical and Process Engineering Research*, vol. 44, pp. 16–25, 2016.

[21] R. Karthik, P. Muthukrishnan, S. M. Chen, B. Jeyaprabha, and P. Prakash, "Anti-corrosion inhibition of mild steel in 1M hydrochloric acid solution by using Tiliacora accuminata leaves extract," *International Journal of Electrochemical Science*, vol. 10, no. 5, pp. 3707–3725, 2014.

[22] R. Lopes-Sesenes, G. G. G.-R. J. Francisca Dominguez-Patino, and A. Marinez-Villafane, "Corrosion inhibition of carbon steel by extract of Buddleia perfoliata," *Journal of Electrochemical Science and Engineering*, vol. 2, pp. 77–90, 2012.

[23] A. M. Al-Mayouf, A. K. Al-Ameery, and A. A. Al-Suhybani, "Inhibition of type 304 stainless steel corrosion in 2M sulfuric acid by some benzoazoles-time and temperature effects," *Corrosion*, vol. 57, no. 7, pp. 614–620, 2001.

[24] D. Daoud, T. Douadi, H. Hamani, S. Chafaa, and M. Al-Noaimi, "Corrosion inhibition of mild steel by two new S-heterocyclic compounds in 1M HCl: experimental and computational study," *Corrosion Science*, vol. 94, pp. 21–37, 2015.

[25] Y. Koumya, R. Idouhli, A. Sayout, A. Abouelfida, A. Benyaich, and A. Romane, "Experimental and theoretical approach on the enhanced inhibitory effect of tetracyclic triterpenes for stainless steel corrosion in sulfuric acid," *Metallurgical and Materials Transactions A*, vol. 50, no. 6, pp. 3002–3012, 2019.

[26] Y. Koumya, R. Idouhli, M. Khadiri et al., "Pitting corrosion and effect of Euphorbia echinus extract on the corrosion behavior of AISI 321 stainless steel in chlorinated acid," *Corrosion Reviews*, vol. 37, no. 3, pp. 259–271, 2019.

[27] R. Idouhli, Y. Koumya, M. Khadiri, A. Aityoub, A. Abouelfida, and A. Benyaich, "Inhibitory effect of Senecio anteuphorbium as green corrosion inhibitor for S300 steel," *International Journal of Industrial Chemistry*, vol. 10, no. 2, pp. 133–143, 2019.

[28] H. Zarrok, A. Zarrouk, B. Hammouti, R. Salghi, C. Jama, and F. Bentiss, "Corrosion control of carbon steel in phosphoric acid by purpald—weight loss, electrochemical and XPS studies," *Corrosion Science*, vol. 64, pp. 243–252, 2012.

[29] R. G. Parr and W. Yang, *Density Functional Theory of Atoms and Molecules*, Oxford University Press, Oxford, UK, 1989.

[30] S. Deng and X. Li, "Inhibition by Jasminum nudiflorum lindl. leaves extract of the corrosion of aluminium in HCl solution," *Corrosion Science*, vol. 64, pp. 253–262, 2012.

[31] H. S. Klapper, J. Goellner, A. Burkert, and A. Heyn, "Environmental factors affecting pitting corrosion of type 304 stainless steel investigated by electrochemical noise measurements under potentiostatic control," *Corrosion Science*, vol. 75, pp. 239–247, 2013.

[32] J.-j. Fu, S.-n. Li, Y. Wang, L.-h. Cao, and L.-d. Lu, "Computational and electrochemical studies of some amino acid compounds as corrosion inhibitors for mild steel in hydrochloric acid solution," *Journal of Materials Science*, vol. 45, no. 22, pp. 6255–6265, 2010.

[33] I. Lukovits, E. Kálmán, and F. Zucchi, "Corrosion inhibitors-correlation between electronic structure and efficiency," *Corrosion*, vol. 57, no. 1, pp. 3–8, 2001.

[34] E. Gutiérrez, J. A. Rodríguez, J. Cruz-Borbolla, J. G. Alvarado-Rodríguez, and P. Thangarasu, "Development of a predictive model for corrosion inhibition of carbon steel by imidazole and benzimidazole derivatives," *Corrosion Science*, vol. 108, pp. 23–35, 2016.

[35] M. Rajendran, K. Keerthika, M. Kowsalya, and D. Devapiriam, "CODEN (USA): PCHHAX theoretical studies on corrosion inhibition efficiency of pyridine carbonyl derivatives using DFT method," *Der Pharma Chemica*, vol. 8, no. 3, pp. 71–79, 2016.

[36] M. Yadav, L. Gope, N. Kumari, and P. Yadav, "Corrosion inhibition performance of pyranopyrazole derivatives for mild steel in HCl solution: gravimetric, electrochemical and DFT studies," *Journal of Molecular Liquids*, vol. 216, pp. 78–86, 2016.

[37] M. S. Masoud, M. K. Awad, M. A. Shaker, and M. M. T. El-Tahawy, "The role of structural chemistry in the inhibitive performance of some aminopyrimidines on the corrosion of steel," *Corrosion Science*, vol. 52, no. 7, pp. 2387–2396, 2010.

[38] J. Saranya, P. Sounthari, K. Parameswari, and S. Chitra, "Adsorption and density functional theory on corrosion of mild steel by a quinoxaline derivative," *Der Pharma Chemica*, vol. 7, no. 8, pp. 187–196, 2015.

[39] M. Olayemi Abdulazeez, A. K. Oyebamiji, A. K. Oyebamiji, and B. Semire, "DFT and QSAR study of corrosion inhibition on 3,5-di-substituted pyrazole derivatives with heteroatom on position one," *Lebanese Science Journal*, vol. 17, no. 2, pp. 217–232, 2016.

[40] L. M. Rodríguez-Valdez, W. Villamisar, M. Casales et al., "Computational simulations of the molecular structure and corrosion properties of amidoethyl, aminoethyl and hydroxyethyl imidazolines inhibitors," *Corrosion Science*, vol. 48, no. 12, pp. 4053–4064, 2006.

[41] N. Boussalah, S. Ghalem, S. El Kadiri, B. Hammouti, and R. Touzani, "Theoretical study of the corrosion inhibition of some bipyrazolic derivatives: a conceptual DFT investigation," *Research on Chemical Intermediates*, vol. 38, no. 8, pp. 2009–2023, 2012.

[42] N. O. Obi-egbedi and I. B. Obot, "Inhibitive properties, thermodynamic and quantum chemical studies of alloxazine on mild steel corrosion in H_2SO_4," *Corrosion Science*, vol. 53, no. 1, pp. 263–275, 2011.

[43] A. Döner, E. A. Şahin, G. Kardaş, and O. Serindağ, "Investigation of corrosion inhibition effect of 3-[(2-hydroxy-benzylidene)-amino]-2-thioxo-thiazolidin-4-one on corrosion of mild steel in the acidic medium," *Corrosion Science*, vol. 66, pp. 278–284, 2013.

[44] A. K. Satpati, M. M. Palrecha, and R. I. Sundaresan, "Electrochemical study of the mechanism of interaction of 1, 2, 3-benzotriazole on SS304 surface in HCl medium," *Indian Journal of Chemical Technology*, vol. 15, pp. 163–167, 2008.

[45] S. A. Umoren, M. J. Banera, T. Alonso-Garcia, C. A. Gervasi, and M. V. Mirífico, "Inhibition of mild steel corrosion in HCl solution using chitosan," *Cellulose*, vol. 20, no. 5, pp. 2529–2545, 2013.

[46] K. Wan, P. Feng, B. Hou, and Y. Li, "Enhanced corrosion inhibition properties of carboxymethyl hydroxypropyl chitosan for mild steel in 1.0M HCl solution," *RSC Advances*, vol. 6, no. 81, pp. 77515–77524, 2016.

[47] P. Preethi Kumari, P. Shetty, and S. A. Rao, "Electrochemical measurements for the corrosion inhibition of mild steel in 1M hydrochloric acid by using an aromatic hydrazide derivative," *Arabian Journal of Chemistry*, vol. 10, no. 5, pp. 653–663, 2017.